Human Molecular Genetics, 2018, Vol. 27, No. 8 1421–1433

doi: 10.1093/hmg/ddy052
Advance Access Publication Date: 8 February 2018
Original Article

ORIGINAL ARTICLE

Loss-of-function and gain-of-function mutations in *PPP3CA* cause two distinct disorders

Takeshi Mizuguchi[1], Mitsuko Nakashima[2], Mitsuhiro Kato[3], Nobuhiko Okamoto[4], Hirokazu Kurahashi[5], Nina Ekhilevitch[6], Masaaki Shiina[7], Gen Nishimura[8], Takashi Shibata[9], Muneaki Matsuo[10], Tae Ikeda[11], Kazuhiro Ogata[7], Naomi Tsuchida[1], Satomi Mitsuhashi[1], Satoko Miyatake[1,12], Atsushi Takata[1], Noriko Miyake[1], Kenichiro Hata[13], Tadashi Kaname[14], Yoichi Matsubara[15,16], Hirotomo Saitsu[2] and Naomichi Matsumoto[1,*]

[1]Department of Human Genetics, Yokohama City University Graduate School of Medicine, Yokohama 236-0004, Japan, [2]Department of Biochemistry, Hamamatsu University School of Medicine, Hamamatsu 431-3192, Japan, [3]Department of Pediatrics, Showa University School of Medicine, Tokyo 142-8666, Japan, [4]Department of Medical Genetics, Osaka Women's and Children's Hospital, Osaka 594-1101, Japan, [5]Department of Pediatrics, Aichi Medical University, Aichi 480-1195, Japan, [6]The Genetics Institute, Rambam Health Care Campus, Haifa 3109601, Israel, [7]Department of Biochemistry, Yokohama City University Graduate School of Medicine, Yokohama 236-0004, Japan, [8]Center for Intractable Diseases, Saitama Medical University Hospital, Saitama 350-0495, Japan, [9]Department of Child Neurology, Okayama University Graduate School of Medicine, Dentistry and Pharmaceutical Sciences, Okayama 700-8558, Japan, [10]Department of Pediatrics, Saga University Faculty of Medicine, Saga 849-8501, Japan, [11]Department of Pediatric Neurology, Osaka Women's and Children's Hospital, Osaka 594-1101, Japan, [12]Clinical Genetics Department, Yokohama City University Hospital, Yokohama 236-0004, Japan, [13]Department of Maternal-Fetal Biology, National Research Institute for Child Health and Development, Tokyo 157-8535, Japan, [14]Department of Genome Medicine, National Center for Child Health and Development, Tokyo 157-8535, Japan, [15]Department of Medical Genetics, Tohoku University School of Medicine, Sendai 980-8574, Japan and [16]National Research Institute for Child Health and Development, Tokyo 157-8535, Japan

*To whom correspondence should be addressed at: Department of Human Genetics, Yokohama City University Graduate School of Medicine, 3-9 Fukuura, Kanazawa-ku, Yokohama 236-0004, Japan. Tel: +81 457872606; Fax: +81 457865219; Email: naomat@yokohama-cu.ac.jp

Abstract

Calcineurin is a calcium (Ca^{2+})/calmodulin-regulated protein phosphatase that mediates Ca^{2+}-dependent signal transduction. Here, we report six heterozygous mutations in a gene encoding the alpha isoform of the calcineurin catalytic subunit (*PPP3CA*). Notably, mutations were observed in different functional domains: in addition to three catalytic domain

Received: December 7, 2017. **Revised:** January 25, 2018. **Accepted:** February 5, 2018

mutations, two missense mutations were found in the auto-inhibitory (AI) domain. One additional frameshift insertion that caused premature termination was also identified. Detailed clinical evaluation of the six individuals revealed clinically unexpected consequences of the *PPP3CA* mutations. First, the catalytic domain mutations and frameshift mutation were consistently found in patients with nonsyndromic early onset epileptic encephalopathy. In contrast, the AI domain mutations were associated with multiple congenital abnormalities including craniofacial dysmorphism, arthrogryposis and short stature. In addition, one individual showed severe skeletal developmental defects, namely, severe craniosynostosis and gracile bones (severe bone slenderness and perinatal fractures). Using a yeast model system, we showed that the catalytic and AI domain mutations visibly result in decreased and increased calcineurin signaling, respectively. These findings indicate that different functional effects of *PPP3CA* mutations are associated with two distinct disorders and suggest that functional approaches using a simple cellular system provide a tool for resolving complex genotype–phenotype correlations.

Introduction

Calcineurin is a heterodimer composed of two subunits: catalytic A (CnA) and regulatory B (CnB) subunits. For full activation of calcineurin, a third component, calmodulin (CaM), binds to CnA (1). This protein complex functions as a serine/threonine-specific protein phosphatase that regulates the phosphorylation status of a large number of downstream targets, including transcription factors, ion channels and cytoskeletal proteins (2). Both CnB and CaM are calcium (Ca^{2+})-binding proteins that activate CnA activity in response to increased intracellular Ca^{2+}. The C-terminal region of CnA contains an auto-inhibitory (AI) domain (3). In an inactive state, the AI domain is thought to interact with the catalytic active site of CnA and inhibit enzyme activity. Binding of Ca^{2+} to the regulatory proteins, CnB and CaM, results in conformational change of CnA that displaces the AI domain from the catalytic active site and leads to full activation of CnA (2,4). Upon activation, CnA dephosphorylates several substrates, including a well-known transcription factor family, nuclear factor of activated T cells (NFAT). Calcineurin can regulate gene expression through NFAT, which normally localizes to the cytoplasm but translocates to the nucleus when dephosphorylated. After its nuclear translocation, NFAT binds to gene promoters and regulates the expression of downstream target genes. As such, calcineurin responds to increased intracellular Ca^{2+} levels to translate this signal for transcriptional regulation via NFAT. Although this pathway is suggested to play a role in the development and/or function of many organ systems, including the immune, nervous, cardiovascular, musculoskeletal and urinary systems (5), evidence of its mutational consequences in humans is limited.

Very recently, a large-scale exome analysis focusing on *de novo* mutations highlighted protein phosphatase 3 catalytic subunit alpha (*PPP3CA*) as a new candidate for neurodevelopmental disorder with epilepsy (6). Although *de novo* mutations of *PPP3CA* were statistically enriched in a large combined cohort, pathogenicity of its mutations and possible genotype–phenotype correlations need to be resolved. Genetic data combined with effective functional studies may provide new insight into the underlying mechanisms and genotype–phenotype correlations.

Here, our group identified *PPP3CA* mutations in six families (five novel and one reported) and extensively assessed their effects on the calcineurin signaling pathway using the fission yeast, *Schizosaccharomyces pombe*, as a model system. Notably, two functionally distinct types of mutations were experimentally demonstrated: loss-of-function and constitutively activating mutations at catalytic and AI domains, respectively. Surprisingly, these two mutational types led to clinically distinct phenotypes. Detailed mutational and clinical features are described here.

Results

Identification of *de novo PPP3CA* mutations

We initially performed trio-based whole-exome sequencing (WES) for Family 1. After filtering, two heterozygous *de novo* variants were identified: c.702C>G (p.Asp234Glu) in *PPP3CA* and c.412G>A (p.Glu138Lys) in *KDM1A* (encodes lysine-specific demethylase 1A). These two variants were not present in dbSNP Build 150, Exome Aggregation Consortium (ExAC) or our in-house Japanese exome controls ($n = 575$ individuals). *PPP3CA* is highly expressed in mammalian brain tissue. The c.702C>G variant was predicted to be pathogenic by four bioinformatic tools: SIFT, Polyphen2, CADD and MutationTaster (Supplementary Material, Table S1). *KDM1A* is expressed in various tissues including the brain, and c.412G>A was deemed pathogenic based on at least two bioinformatic tools (Polyphen2 and MutationTaster). These two genes are potentially causal in the family. Next, we searched for *PPP3CA* or *KDM1A* mutations in our WES datasets of cases with epilepsy ($n = 1456$) to identify unrelated individuals with potential variants in these genes. We identified four additional rare variants in *PPP3CA* but none in *KDM1A*. Thus, altogether we identified five rare variants in *PPP3CA* (four missense and one frameshift). Four of them occurred *de novo* and were confirmed by Sanger sequencing: c.702C>G (p.Asp234Glu), c.275A>G (p.His92Arg), c.1290dupC (p.Met431Hisfs*20) and c.1417G>A (p.Ala473Thr) in Families 1, 3, 4 and 6, respectively (Fig. 1A). In Family 2, paternal DNA was unavailable and maternal inheritance of c.449A>T (p.Asn150Ile) was ruled out (Fig. 1A). Constraint metrics in ExAC showed that *PPP3CA* is under constraint for missense (Z score = 3.89) and loss-of-function [probability of being loss-of-function intolerant (pLI) = 1.00] variants. This evidence strongly supports the pathogenicity of *PPP3CA* variants. In functional studies of these variants, Myers *et al.* reported significant enrichment of *de novo* *PPP3CA* variants in neurodevelopmental disorders by exome and targeted sequencing analysis of 4760 trios (6). Collectively, these findings suggest that *de novo* heterozygous variants in *PPP3CA* can cause epilepsy.

PPP3CA functional domains, mutations and clinical features

PPP3CA contains one catalytic and three regulatory domains, including calcineurin B binding (CnBB), calmodulin binding (CaMB) and AI domains (Fig. 1B). Of three missense variants at the catalytic domain, p.His92Arg and p.Asn150Ile (but not p.Asp234Glu) are present in metal binding sites of the phosphoesterase motif (1) (Fig. 1B). All three catalytic domain variants altered evolutionarily conserved amino acids from human to yeast, and were predicted to be pathogenic by SIFT,

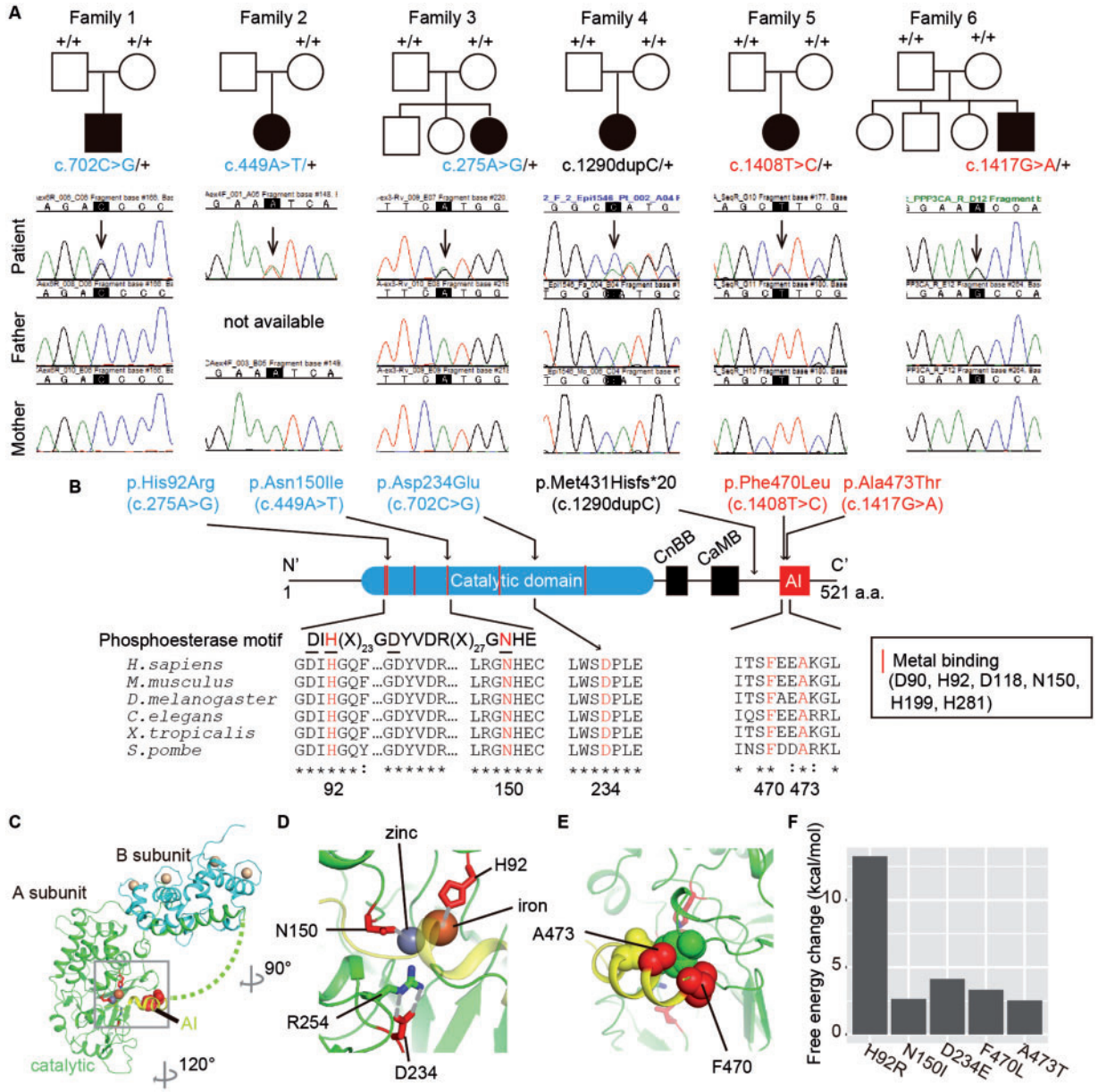

Figure 1. *PPP3CA* mutations identified in this study. (**A**) Family pedigrees and *PPP3CA* mutations. Arrows in electropherograms indicate heterozygous mutations. (**B**) Functional domains of PPP3CA with a summary of the mutations. Mutation sites are shown above the PPP3CA protein. CnBB, calcineurin B-binding domain; CaMB, calmodulin-binding domain and AI, auto-inhibitory domain. The six metal-ion binding sites to dinuclear metal cofactors are highlighted as red bars on PPP3CA protein. Blue, catalytic domain mutations; red, AI domain mutations; black, frameshift mutation (top). Phylogenetic conservation of amino acid residues altered by mutation (bottom). Metal-ion binding sites in the phosphoesterase motif are underlined. (**C**) Evaluation of effects of mutation on protein structure. Crystal structure of human calcineurin heterodimer (PDB code, 1AUI) is shown. Catalytic and AI domains are colored green and yellow, respectively, with the B subunit colored cyan. Calcium, zinc and iron ions are shown as spheres in beige, deep blue and orange, respectively. Residues at mutation sites His92, Asn150 and Asp234 are shown as red sticks, while Phe470 and Ala473 are shown as van der Waals spheres in red. The green dotted region represents the missing region of the A subunit (aa residues 374–413). (**D, E**) Enlarged view of the region enclosed by the gray rectangle is shown from different angles. The α-helix of the AI domain is displayed as translucent, while the gray solid and dotted lines depict coordinate and hydrogen bonds, respectively. Molecular structures were drawn with PyMOL (www.pymol.org). (**F**) Free energy changes with identified *PPP3CA* mutations calculated by FoldX software.

Polyphen2, CADD and MutationTaster (Supplementary Material, Table S1). Individuals with catalytic domain mutations showed similar clinical manifestations. They had non-syndromic epileptic encephalopathy with spasms and hypsarrhythmia as determined by electroencephalography (EEG), leading to a clinical diagnosis of West syndrome (Table 1, Supplementary Material, Figs S1 and S2). One additional frameshift variant, c.1290dupC (p.Met431Hisfs*20), was also identified in an individual with nonsyndromic epileptic encephalopathy (Table 1). Her initial diagnosis was also West syndrome. These observations suggest that these variants have a similar impact on PPP3CA function and cause early onset epileptic encephalopathy.

We also identified a *de novo* missense variant (c.1417G>A, p.Ala473Thr) at the AI domain (aa 465–487 based on UniProtKB: Q08209) in a boy who showed not only developmental delay with seizure but also dysmorphic features, including trigonocephaly,

Table 1. Clinical features of individuals with *PPP3CA* mutations

Family		1 (Patient 1)	2 (Patient 2)	3 (Patient 3)	4 (Patient 4)	5 (Patient 5)	6 (Patient 6)
Age		2 y	19 y	4 y	2 y	5 y	7 y
Gender		M	F	F	F	F	M
Mutation		c.702C>G (p.Asp234Glu)	c.449A>T (p.Asn150Ile)	c.275A>G (p.His92Arg)	c.1290dupC (p.Met431Hisfs*20)	c.1408T>C (p.Phe470Leu)	c.1417G>A (p.Ala473Thr)
Inheritance		*de novo*	N.D.	*de novo*	*de novo*	*de novo*	*de novo*
Clinical diagnosis		WS	WS, LGS, and RS	WS	EE	MCA/ID (OCS like)	DD with seizures
Gestation (weeks)		40	38	38	36	37	37
Birth weight (g)		3790	2826	3058	2344	3098	2815
Birth length (cm)		N.D.	N.D.	48	47	39	34
Height (SD)		−0.1 SD	−1.5 SD	−2.0 SD	−1.7 SD	−4.4 SD	−5 SD
Weight (SD)		−1.8 SD	−1.9 SD	−0.5 SD	−2.9 SD	−2.9 SD	−4 SD
OFC (SD)		−0.2 SD	−2.3 SD	N.D.	+0.1 SD	+1.9 SD	−3.5 SD
Seizure	Age of onset	7 m	8 m	22 m	6 m	−	9 m
	Seizure type (onset)	ES and M	ES	ES	ES	−	G
	EEG	Hypsarrhythmia at 10 m, multifocal epileptic discharge at 25 m	Hypsarrhythmia at 8 m, diffuse spike-and-slow waves and polyspike-and-slow waves at 10 y	Occipital polyspike-and-slow waves at 2 y	Hypsarrhythmia at 7 m, repetitive diffuse polyspike-slow waves at 25 m	−	Abnormal background activity without epileptic discharge at 1 y and 4 y
	Seizure type (last visit)	ES	T, At, and Ab	ES	FS and ES	−	G
	Seizure prognosis	Intractable	Intractable	Intractable	Intractable	−	Tractable
Development	DD	+	+	+	+	+	+
	DQ	7 at 25 m	<10 at 19 y	27 at 2 y	N.D.	<10	50
Neurological	Hypotonic quadriplegia	+	+	−	+	−	−
	Intellectual disability	Profound	Profound	Severe	Severe	Severe	Moderate
	Stereotypical behavior	+	+	−	−	−	+
Dysmorphism	Craniosynostosis	−	−	−	−	+ (Plagiocephaly)	+ (Trigonocephaly)
	Micro- and retrognathia	−	−	−	−	+	+
	Cleft palate	−	−	−	−	+	+
	Brachydactyly	−	−	−	−	+	+
Delayed calvarial ossification		−	−	−	−	+	N.D.
Skeletal	Gracile bones	−	−	−	−	+	N.D.
	Pathogenic fractures	−	−	−	−	+	−
	Arthrogryposis	−	−	−	−	+	+
Renal	Hydronephrosis	−	−	−	−	+	−
	VUR	−	−	−	−	+	−

cDNA and protein changes are based on reference cDNA, NM_000944.4. Abbreviations: +, present; −, absent; M, male; F, female; y, years; m, months; N.D.: not determined; OFC, occipitofrontal circumference; Ab, atypical absence seizure; At, atonic seizure; DQ, developmental quotient; ES, epileptic spasm; FS, focal seizure; G, generalized seizure; M, myoclonus; T, tonic seizure; VUR, vesicoureteral reflux; DD, developmental delay; EE, epileptic encephalopathy; LGS, Lennox–Gastaut syndrome; MCA/ID, multiple congenital anomalies/intellectual disability; OCS, osteocraniostenosis; RS, Rett syndrome; WS, West syndrome.

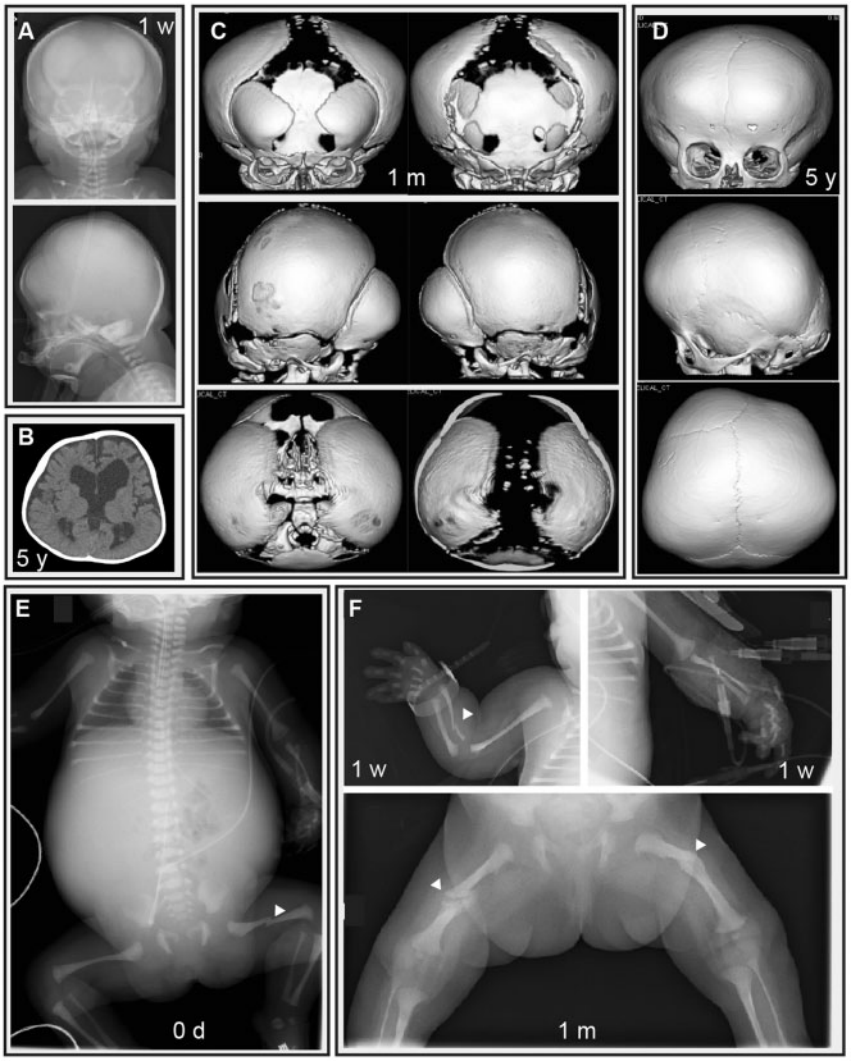

Figure 2. Clinical features of an individual with AI domain mutation (family 5). (**A–C**) Neonatal skull radiographs, brain CT and three-dimensional CT showed brachycephaly with wide cranial sutures, ventriculomegaly and narrowing of the inferior segment of coronal sutures. (**D**) Three-dimensional CT at 5 years of age showed frontal plagiocephaly due to complete synostosis of the left coronal suture. (**E, F**) Neonatal skeletal survey showed a gracile form of the ribs and tubular bones, fracture of the left femur, with later development of fractures of the right radius and right femur (arrowheads).

cleft palate, micrognathia and brachydactyly (patient 6). Other hallmarks comprised arthrogryposis and a short stature (Table 1). This distinctive phenotype prompted us to search for *PPP3CA* variants in our other study cohorts, focusing on patients with intellectual disability and multiple congenital anomalies (ID/MCA). As a result, we identified another *de novo* AI domain variant (c.1408T>C, p.Phe470Leu) in a girl (patient 5). These two patients (5 and 6) shared several features including craniosynostosis, cleft palate, micrognathia, arthrogryposis and short stature, but their facial features were not similar (Supplementary Material, Fig. S3). Unlike patient 6, patient 5 showed severe slenderness of the ribs and tubular bones, and perinatal fractures (gracile bones) (Fig. 2A–F). Moreover, craniosynostosis was more overt in patient 5 than in patient 6. In contrast, patient 6 exhibited developmental delay with seizures. The phenotype of patient 5 was reminiscent of osteocraniostenosis, an autosomal dominant disorder arising from mutations in family with sequence similarity 111 member A (*FAM111A*) (7). However, *FAM111A* was normal in our exome data (mean coverage of *FAM111A* coding sequence was 117.18×, with at least 96% of target bases sequenced by ≥ 20 reads). Based on patients 5 and 6, we re-evaluated extra-neurological findings in individuals with catalytic domain mutations but did not find even subtle dysmorphic signs in any individuals except for microcephaly in patient 2. Thus, developmental delay and ID/MCA are likely to be associated with mutations at the AI domain. These clinical manifestations are summarized in Table 1, with case reports presented in the Materials and Methods section. In summary, we suggest that *PPP3CA* variants in different functional domains (catalytic versus AI domains) cause two distinct (allelic) disorders.

Structural impact of five missense variants

To evaluate the impact of the identified mutations on human calcineurin structure, we mapped mutation sites onto the crystal structure of human calcineurin heterodimer (PDB code: 1AUI) (8). In this structure, the AI domain interacts with the catalytic center (Fig. 1C). Residues at the mutation sites, His92 and Asn150, correspond to the catalytic ions, iron and zinc, respectively. Thus, p.His92Arg and p.Asn150Ile mutations may impair correct folding and enzymatic activity. The Asp234 side chain

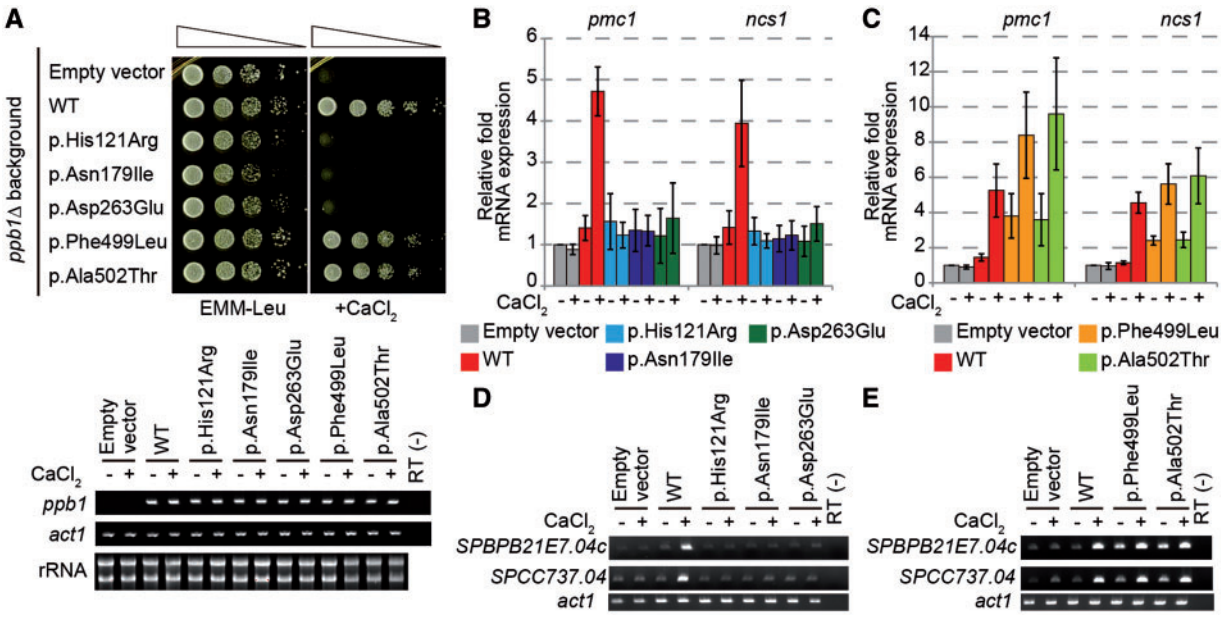

Figure 3. Functional studies using a yeast model system. (**A**) Calcium intolerance was rescued by overexpression of wild-type and AI domain mutants, but not catalytic domain mutants (p.His121Arg, p.Asn179Ile, p.Asp263Glu, p.Phe499Leu and p.Ala502Thr correspond to human p.His92Arg, p.Asn150Ile, p.Asp234Glu, p.Phe470Leu and p.Ala473Thr, respectively). Ten-fold serial dilutions of each strain were spotted onto EMM minimal medium with or without 200 mM $CaCl_2$ (final concentration). Cells were grown at 32°C for 5 days. pREP1 vector containing *S. cerevisiae LEU2* as a selectable marker was used for overexpression of wild-type and mutant *ppb1* on a *ppb1* deletion strain background. Ectopic expression of *ppb1* was validated by RT-PCR. *act1* was used as a control. RT (−), no reverse transcription. (**B**, **C**) Transcriptional dysregulation by catalytic and AI domain mutations. Real-time RT-PCR was performed using the indicated strains. *pmc1* or *ncs1* expression was normalized by *act1*, and then further relative to an untreated sample (empty vector without $CaCl_2$). Error bars indicate SD from three biological replicates. (**D**, **E**) RT-PCR analysis of *SPBPB21E7.04c* and *SPCC737.04* expression levels in the indicated strains. *act1* was used as a control. RT (−), no reverse transcription. Representative data are shown from biological triplicate experiments.

forms hydrogen bonds with Arg254, which is highly conserved among species and reportedly positioned to bind phosphate oxygen in the substrate (8) (Fig. 1D). Thus, catalytic activity is predicted to be impaired when Asp234 is replaced with a glutamate residue, which has a slightly longer side chain than that of an aspartate residue. Phe470 and Ala473 in the α-helix of the AI domain were located at the surface involved in the interaction between the AI domain and the catalytic domain with the hydrophobic core (Fig. 1E). Consequently, p.Phe470Leu and p.Ala473Thr mutations are likely to destabilize the interaction between AI and catalytic domains, leading to impaired autoinhibition of catalytic activity by the AI domain. We also calculated the change in free energy of each mutation using FoldX software 2 (9) (Fig. 1F). All tested mutations showed at least 2 kcal/mol increases in free energy, potentially leading to instability of protein folding and supporting our above discussion.

Functional relevance of *PPP3CA* mutations

In silico modeling suggested that both catalytic and AI domain mutations affected the domain structure or overall folding of PPP3CA. To study the functional effects of these variants, we used the fission yeast *S. pombe* as a model system for examining calcineurin signaling. The *ppb1* gene encodes a calcineurin catalytic subunit (CnA) in *S. pombe* (10). The amino acid sequence of *ppb1* was 63% identical to that of human *PPP3CA* with a highly conserved primary domain structure (Supplementary Material, Fig. S4). *Ppb1* is not an essential gene but is required for viability in specific growth conditions such as those with high extracellular Ca^{2+}. As previously shown (11), the *ppb1* deletion strain (*ppb1*Δ) grows well under standard conditions but has a growth defect in high-Ca^{2+} conditions (Fig. 3A). Full-length *ppb1* cDNA was cloned into the *S. pombe* expression vector, pREP1, and transformed into *ppb1*Δ. Ten-fold serial dilution of a yeast strain ectopically expressing wild-type *ppb1* was spotted and grown at 32°C. As expected, the Ca^{2+}-hypersensitive phenotype was fully rescued by ectopic expression of wild-type *ppb1* but not empty vector (Fig. 3A). Accordingly, this assay enabled us to evaluate the *in vivo* function of mutant proteins. In mammalian cells, response to Ca^{2+} influx triggered by synaptic neurotransmission is crucial for proper neuronal activity (12). From this perspective, evaluating the function of proteins in Ca^{2+} tolerance might be appropriate for characterizing variants of unknown significance. Expression plasmids were constructed encoding the three catalytic and two AI domain *ppb1* mutations (p.His121Arg, p.Asn179Ile, p.Asp263Glu, p.Phe499Leu and p.Ala502Thr correspond to human p.His92Arg, p.Asn150Ile, p.Asp234Glu, p.Phe470Leu and p.Ala473Thr, respectively). Mutant *ppb1* was overexpressed in *ppb1*Δ and its growth was compared with that of cells transformed with wild-type *ppb1*. Although wild-type and mutant forms of *ppb1* were overexpressed (Fig. 3A), all three catalytic domain mutations (p.His121Arg, p.Asn179Ile and p.Asp263Glu) failed to rescue the Ca^{2+}-sensitive phenotype, suggesting that they are all loss-of-function mutations. In contrast, yeast cells overexpressing AI domain mutations (p.Phe499Leu and p.Ala502Thr) rescued Ca^{2+} sensitivity, similar to wild-type *ppb1*. This indicates that AI domain mutations affect calcineurin signaling differently from catalytic domain mutations.

Transcriptional dysregulation by catalytic and AI domain mutations

AI domain mutations were associated with the retention of function, at least with respect to Ca^{2+} tolerance. To determine how AI domain mutations cause ID/MCA, we examined

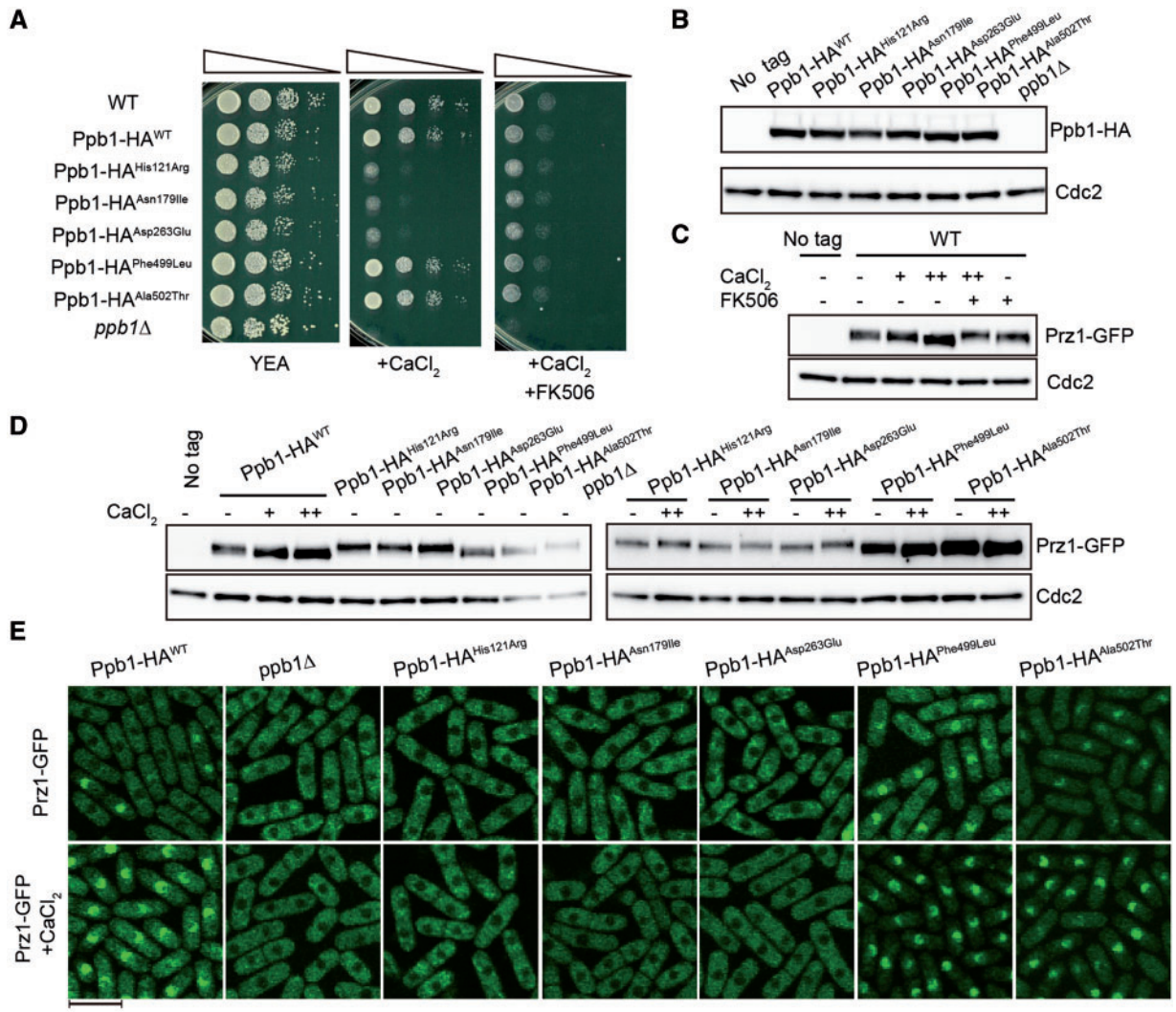

Figure 4. Enzymatic action of catalytic and AI domain mutations to transcription factor Prz1. (**A**) Ten-fold serial dilutions of each strain were spotted on the indicated YEA-rich medium. Cells were grown at 32°C for 3 days. (**B**) Western blotting showing expression of endogenous C-terminal HA-tagged wild-type and mutant Ppb1. (**C**) Western blotting showing mobility shift of Prz1. Cells expressing endogenous C-terminal GFP-tagged Prz1 were treated for 30 min with $CaCl_2$ (+, 100 mM; ++, 200 mM final concentration) either alone or with FK506 (0.5 μg/ml). (**D**) Western blotting showing Prz1 migration on SDS-PAGE gels using extract from the indicated strains. Cdc2 was used as a loading control in Figure 4B–D. (**E**) Live-cell imaging of Prz1-GFP. Cells expressing Prz1-GFP were cultured at 32°C for 30 min in the presence of 200 mM $CaCl_2$. A representative image from biological duplicate experiments is shown. Scale bar, 10 μm.

calcineurin signaling at the molecular level. When yeast cells were exposed to a high concentration of extracellular Ca^{2+}, several downstream genes, including *ncs1* (encodes neuronal calcium sensor 1) and *pmc1* (encodes vacuolar calcium transporting P-type ATPase P2 type), were upregulated for Ca^{2+} homeostasis (11,13). This Ca^{2+}-induced transcriptional regulation is mediated by calcineurin. To distinguish the functional impact of catalytic and AI domain mutations at the transcriptional level, we monitored *ncs1* and *pmc1* expression by real-time PCR. When wild-type *ppb1* was overexpressed, both *pmc1* and *ncs1* were upregulated after Ca^{2+} stimulation, showing activation of the calcineurin signal (Fig. 3B). Consistent with the lack of growth rescue by dilution assay (Fig. 3A), transcriptional upregulation of *ncs1* and *pmc1* was not observed with the three catalytic domain mutants (Fig. 3B). Interestingly, derepression of calcineurin signaling was consistently observed with the two AI domain mutants, as indicated by increased expression of both *pmc1* and *ncs1* without Ca^{2+} stress (Fig. 3C). Similar observations were found with other downstream target genes of calcineurin, such as *SPBPB21E7.04c* and *SPCC737.04* (14), suggesting that a pleiotropic (or even generalized) phenotype is potentially produced by AI domain mutations (Fig. 3D and E).

Enzymatic effects of catalytic and AI domain mutations

The basic mechanism of the calcineurin–NFAT signal is conserved in the yeast model system. Transcriptional upregulation of *pmc1* and *ncs1* is mediated by a calcineurin-activated transcription factor, Prz1. Prz1 is dephosphorylated by calcineurin and translocates from the cytoplasm to the nucleus for transcriptional regulation (11). Transcriptional dysregulation (Fig. 3B–E) of catalytic and AI domain mutants suggests that the phosphatase activity of calcineurin might be affected by missense mutations. To study changes in calcineurin phosphatase function, we investigated the activation status of Prz1.

First, we generated a yeast strain endogenously expressing C-terminal HA-tagged Ppb1 (Ppb1-HA^{WT}). This strain was not sensitive to Ca^{2+}, indicating that the fusion protein is functional (Fig. 4A). We next mutated the corresponding amino acid residues of endogenously expressed Ppb1-HA (Ppb1-HA^{His121Arg}, Ppb1-HA^{Asn179Ile}, Ppb1-HA^{Asp263Glu}, Ppb1-HA^{Phe499Leu} and Ppb1-HA^{Ala502Thr}). Western blotting showed comparable protein levels between Ppb1 mutants and the wild type, suggesting that catalytic and AI domain mutations do not affect protein stability (Fig. 4B). Consistent with a loss-of-function effect in rescue experiments (Fig. 3A), Ppb1-HA catalytic domain mutants showed hypersensitivity to high Ca^{2+} levels, similar to *ppb1*Δ. The same levels of Ca^{2+} sensitivity were obtained by pharmacological inhibition of calcineurin activity using FK506 (FK506-treated wild-type cells versus catalytic domain mutants). These observations suggest that catalytic domain mutants are functionally null with respect to enzymatic action (Fig. 4A).

To directly confirm this possibility, we studied Prz1 modification. The *prz1* gene was chromosomally tagged with GFP at an endogenous locus on the wild-type and *ppb1* mutant backgrounds. The phosphorylation status of Prz1 could be identified by a mobility shift on SDS-PAGE gels followed by western blotting. Consistent with previous reports (11), Prz1 showed slower and faster migration in the absence and presence of Ca^{2+}, respectively (Fig. 4C). Ca^{2+}-induced mobility shift was inhibited by FK506 treatment, suggesting that this change is indeed related to calcineurin activity (Fig. 4C). We then tested whether catalytic domain mutations were associated with defective Prz1 modification. Unlike wild-type cells, Prz1 did not show a mobility shift with catalytic domain mutants after Ca^{2+} stress, indicating that *ppb1* is enzymatically inactive (Fig. 4D). This conclusion was supported by live-cell imaging showing that Prz1 does not translocate to the nucleus in high-Ca^{2+} conditions (Fig. 4E). In contrast to catalytic domain mutants, we found that Prz1 of AI domain mutants migrated faster than either wild-type or catalytic domain mutants in the absence of Ca^{2+} stress (Fig. 4D). Consistent with this, the proportion of cells showing nuclear translocation increased in AI domain mutants without Ca^{2+} stimulation (Fig. 4E). These observations fit the model that AI domain mutations cause transcriptional derepression. Collectively, these results indicate that catalytic and AI domain mutations are enzymatically inactive and constitutively active, respectively.

PPP3CA expression and alternative splicing in fetal and adult brain tissue

Functional studies suggested that the catalytic domain mutations identified here are loss-of-function mutations. Patient 4, who had a frameshift mutation [c.1290dupC (p.Met431Hisfs*20)], presented a clinical picture similar to that of patients with catalytic domain mutations, which suggests a shared underlying pathological mechanism. Hence, we checked whether mutant transcripts were subject to nonsense-mediated mRNA decay (NMD) (15). Transcript analysis was performed using a patient-derived (patient 4) lymphoblast cell line (LCL) (Supplementary Material, Fig. S5). Abundant *PPP3CA* was expressed from both alleles, with the expression levels of the mutated allele not being significantly changed after cycloheximide (CHX) treatment. This suggests that mutated transcripts are unlikely to be subjected to NMD (Supplementary Material, Fig. S5B). However, multiple transcript variants are registered for *PPP3CA*. Therefore, we examined the pattern of *PPP3CA* transcripts in a human tissue panel of cDNA libraries. Two alternative splicing products, transcript variants 1 and 2, were recognized (Supplementary Material, Fig. S5C–E). In an LCL, variant 2 was predominantly expressed. Intriguingly, transcript variant 1 (NM_000944.4) was predominant in the brain and its relative abundance appeared to increase during brain development (Supplementary Material, Fig. S5C–E), suggesting that transcript variant 1 is biologically relevant for evaluating pathogenicity. The c.1290dupC mutation resulted in a premature termination codon (PTC) within the last exon of transcript variant 2 (NM_001130691.1) and penultimate exon of transcript variant 1 (NM_000944.4) (Supplementary Material, Fig. S5A). Taking these findings together, transcript analysis from other tissues expressing transcript variant 1 (including brain or skeletal muscle) may be appropriate to confirm pathological consequences regarding NMD.

Cellular response to drugs

Our experimental results showed that the catalytic and AI domain mutations differentially impact calcineurin signaling, which in turn affects cellular phenotype, namely, Ca^{2+} intolerance. Accordingly, we investigated whether the cellular response to drugs/chemicals/peptides might also be different. We found that mutant yeast strains with catalytic but not AI domain mutations showed hypersensitivity to valproic acid (Supplementary Material, Fig. S6).

Discussion

In this study, we identified six disease-causing mutations in *PPP3CA*. We also demonstrated that mutations within two functional domains affect protein function in distinct ways, which may lead to different clinical phenotypes.

Individuals with catalytic domain mutations (p.His92Arg, p.Asn150Ile and p.Asp234Glu) were clinically diagnosed with West syndrome. Two of three catalytic domain mutations (p.His92Arg and p.Asn150Ile) were located at metal binding sites. Hence, West syndrome may be caused by metal binding site mutations. Consistent with this, two unrelated individuals with metal binding site mutations (p.His92Arg and p.His281Gln) reported by Meyers *et al.* also had West syndrome or Lennox–Gastaut syndrome (6). Although the third mutation, p.Asp234Glu, is not located at a metal binding site, yeast studies indicated that this was also a loss-of-function mutation, similar to p.His92Arg and p.Asn150Ile. Therefore, we suggest that loss-of-function (or null) mutations are associated with West syndrome, regardless of their position within the functional domain. Nonetheless, mutations in the catalytic domain are not always functionally null. Two reported pathogenic mutations (6), p.His281Gln and p.Glu282Lys, are positioned adjacent to each other (Supplementary Material, Fig. S7A) and predicted to be pathogenic by three (SIFT, Polyphen2 and MutationTaster) and four (SIFT, Polyphen2, CADD and MutationTaster) bioinformatic tools, respectively (Supplementary Material, Table S2). Like other metal binding site mutations, p.His281Gln (p.His310Gln in *S. pombe ppb1*) causes West syndrome and is functionally null regarding Ca^{2+} tolerance in a yeast assay (Supplementary Material, Fig. S7B and C). However, p.Glu282Lys (p.Glu311Lys in *S. pombe ppb1*) maintains Ca^{2+} tolerance, similar to wild-type *ppb1* (Supplementary Material, Fig. S7B and C). Interestingly, two different patients with p.Glu282Lys mutations showed developmental delay with dysmorphic features. Further, the seizure type was distinct from West syndrome (i.e. mild and

tractable) in one patient, with no seizures observed in the other patient (6). Such functional differences between mutations might be associated with phenotypic differences in patients with catalytic domain mutations.

AI domain mutations were associated with multiple congenital abnormalities. Two patients with AI domain mutations shared certain clinical features, including developmental delay, craniosynostosis, cleft palate, micrognathia, arthrogryposis and short stature. However, patient 5 distinctively showed gracile bones, as well as markedly severe craniosynostosis. This phenotype is reminiscent of osteocraniostenosis arising from heterozygous *FAM111A* mutations. Nevertheless, patient 5 did not have a *FAM111A* mutation nor other hallmark of osteocraniostenosis (such as ocular malformations, splenic hypoplasia and hypocalcemia). In contrast, patient 5 exhibited arthrogryposis (congenital multiple joint contractures), which is not seen in osteocraniostenosis (7). Severe fetal hypokinesia may create slender bones with or without intrauterine fractures (16). Therefore, this patient's gracile bones may have been a secondary consequence of the fetal hypokinesia sequence, and not an essential syndromic component. Alternatively, calcineurin signaling might have *in vivo* effects on skeletal bone development in humans. In fact, it was reported that calcineurin/NFAT signaling is probably involved in bone remodeling in mice (17,18). Such a bone phenotype might be influenced by environmental and/or genetic modifiers. More studies are needed to establish the clinical features of patients with AI domain mutations.

In this study, we observed tissue-specific alternative splicing of *PPP3CA*, which may affect mutational consequences. In general, NMD is inefficient when PTC occurs at the last exon or last <50 bp of the penultimate exon (19). In patient 4, PTC occurs in the penultimate exon (exon 13) of transcript variant 1. Meyers *et al.* reported *PPP3CA* non-sense mutation (c.1333C>T, p.Gln445*) at exon 12 of transcript variant 1, which is more upstream than the PTC position of our patient 4's mutation (p.Met431Hisfs*20). However, the PTC positions of both mutations were supposed to be located within the <50 bp region from the last exon–exon junction as exon 13 is too short (only 30 bp) and may escape from NMD in brain-specific transcript variant 1. If NMD is inefficient, as with variant 2 in LCL, a dominant-negative and/or gain-of-function effect might be a possible mechanism. However, we cannot fully rule out the possibility that tissue-specific NMD may degrade mutant transcripts in the brain and lead to a haploinsufficient phenotype, similar to catalytic domain mutations. In fact, many exceptions have been reported that do not follow the general rules for NMD efficiency (20–22). The precise mechanism of these two mutations has yet to be proved.

Numerous genes with different functions cause West syndrome. It remains possible that certain treatments will be more effective in specific subtypes, for example, vigabatrin for tuberous sclerosis complex patients (23). In our yeast study, CnA catalytic domain but not AI domain mutants were hypersensitive to an anti-epileptic drug, valproic acid (Supplementary Material, Fig. S6). As such, *PPP3CA*–epileptic encephalopathy might exhibit a unique pharmacological cellular response. The therapeutic response is definitely more complicated and it is not easy to predict drug effectiveness based on the data from experiments using a unicellular organism. Indeed, two patients partially responded to valproic acid (patients 1 and 4), while the others did not (patients 2 and 3). However, future efforts based on pathophysiological mechanisms may lead to better therapeutic strategies. Molecules downstream of calcineurin signaling might be potentially pharmacological targets (24).

In summary, we have provided evidence for the involvement of calcineurin in the pathogenesis of different human phenotypes. Loss-of-function and gain-of-function mutations of *PPP3CA* lead to early onset epileptic encephalopathy and multiple congenital abnormalities, respectively. These two allelic conditions may be derived from the differing nature of *PPP3CA* mutations. This study clearly indicates that functional evaluation of mutations is important for understanding new pathogenic mechanisms and clear genotype–phenotype correlations.

Materials and Methods

Case reports

Patient 1 was the first child of unrelated healthy parents. He was born at 40 weeks of gestation after an uneventful pregnancy. Phototherapy was used for 3 days to treat neonatal jaundice. At the age of 6 months, he was referred to our hospital as no head control had been acquired. Routine blood chemistry was normal except for mild elevation of liver transaminase [aspartate transaminase (AST)/alanine transaminase (ALT), 84/50 IU/L]. Brain CT was normal. Chromosomal karyotype was 46, XY. He showed head nodding or spasm-like movements at 7 months, and their frequency gradually increased and they appeared in clusters. At 10 months of age, he showed profound developmental delay. His developmental quotient (DQ) was 14 (based on the Japanese Enjoji scale for infantile development) and interictal EEG showed hypsarrhythmia (Supplementary Material, Fig. S1A), leading to a diagnosis of West syndrome. Myoclonic seizures were observed on ictal video EEG as well as epileptic spasms. Brain MRI showed frontal-dominant mild brain atrophy (Supplementary Material, Fig. S2A and B). Other laboratory examinations were all normal, including blood chemistry, lactate and pyruvate in cerebrospinal fluid, plasma amino acids, serum acylcarnitine, urine organic acids, visual evoked potential and auditory brainstem response. His seizures on EEG transiently disappeared after 25 days of adrenocorticotropic hormone (ACTH) injection, but high-amplitude epileptic discharges remained at bilateral occipital lobes on EEG. These partially responded to valproic acid, but the adverse effect of thrombocytopenia prevented an increase in dose. At 14 months of age, the epileptic spasms in clusters relapsed, and were refractory to multiple anti-epileptic drugs, such as pyridoxal phosphate, zonisamide, clobazam, topiramate, lamotrigine and a modified Atkins/ketogenic diet. At 25 months of age, he still had epileptic spasms in clusters twice a day. His height was 86.0 cm (−0.1 SD), weight 9.7 kg (−1.8 SD) and head circumference 48.0 cm (−0.2 SD). He showed profound developmental delay (DQ 7 in the Japanese Enjoji scale), hypotonic quadriplegia, unstable head control, no eye contact and no meaningful words. His EEG showed frontal-dominant multifocal epileptic discharges with increased frequency and generalization during the sleep state (Supplementary Material, Fig. S1B).

Patient 2 was born by spontaneous delivery at 38 weeks of gestation after an uneventful pregnancy. She obtained head control at 4 months of age, but acquired social smiling at 5 months of age, indicating developmental delay. At 8 months of age, she developed daily epileptic spasms in clusters with hypsarrhythmia on EEG, leading to a diagnosis of West syndrome. ACTH injection therapy was temporarily effective for her seizures with a partially improved EEG; however, multiple types of generalized seizures (including tonic seizures, atonic seizures and atypical absence seizures) appeared daily. These were refractory to multiple anti-epileptic drugs such as pyridoxal

phosphate, valproic acid, clonazepam, nitrazepam, levetiracetam and acetazolamide. Some anti-epileptic drugs, such as clobazam, phenytoin, zonisamide, topiramate, lamotrigine and potassium bromide, were partially effective against the seizures. Her EEG frequently showed diffuse spike-and-slow waves and polyspike-and-slow waves (Supplementary Material, Fig. S1C), which were compatible with a diagnosis of Lennox–Gastaut syndrome. She had characteristic features of Rett syndrome such as autistic behavior, hand stereotypies (e.g. hand wringing), and tooth grinding. At 19 years of age, her height was 150.4 cm (−1.5 SD), weight 38.5 kg (−1.9 SD) and head circumference 52.4 cm (−2.3 SD). She showed profound ID with no meaningful words. She could roll over by herself but could not sit alone. Head CT at 7 months of age showed no calcification. MRI at 2 years of age showed mild brain atrophy, but this was normal by 8 years of age (Supplementary Material, Fig. S2C and D). EEG at 19 years of age showed frequent diffuse polyspike-and-slow waves during the sleep state (Supplementary Material, Fig. S1D).

Patient 3 was the third child born to unrelated healthy parents. She was born spontaneously at 38 weeks of gestation with no asphyxia. She was referred to our hospital at 16 months because of developmental delay, namely, eye pursuit of an object at 3 months of age, social smiling at 4 months, head control at 5 months and sitting without support at 14 months. She had monthly epileptic spasms at 22 months of age, and the frequency of her seizures increased on a weekly basis at 2 years of age. Video EEG demonstrated epileptic spasms in clusters, with polyspike-and-slow waves at the occipital area and right dominancy during the sleep state (Supplementary Material, Fig. S1E). Her seizures were refractory to ACTH injection and multiple anti-epileptic drugs such as valproic acid, clobazam and zonisamide. Lamotrigine partially reduced the frequency of her seizures. She showed neither dysmorphisms nor involuntary movements. Her DQ was 27 (Kyoto Scale of Psychological Development) at 2 years and 8 months of age. At 3 years and 10 months, her height was 91 cm (−2.0 SD) and body weight 14 kg (−0.5 SD). She could walk with support but was unable to speak meaningful words. Her brain MRI was normal at 17 months and head CT showed no calcification. Mild dilatation of sulci and lateral ventricles was detected immediately after ACTH injection therapy at 2 years and 8 months but had normalized by 4 years of age (Supplementary Material, Fig. S2E and F). EEG findings changed during her development: no paroxysmal discharge at 2 years and 5 months, bilateral frontopolar sharp waves at 2 years and 7 months (Supplementary Material, Fig. S1F), and focal polyspike-and-slow waves at the left occipital region at 3 years and 6 months.

Patient 4 is a 2-year-old girl, who was the first child born to healthy nonconsanguineous parents with no anomalies. She experienced epileptic spasms at 6 months of age. EEG showed hypsarrhythmia (Supplementary Material, Fig. S1G) and brain MRI was unremarkable (Supplementary Material, Fig. S2G and H). She was treated with ACTH, which was effective, but the epileptic spasms recurred immediately after stopping this treatment. At 9 months of age, she experienced focal seizures. Loss of consciousness, eye deviations to the right or the left and ipsilateral hemiconvulsions lasting for a minute were observed weekly. The seizures became intractable despite the administration of various anti-epileptic drugs including clonazepam, zonisamide, topiramate, levetiracetam, carbamazepine, perampanel, pyridoxal phosphate and repeated ACTH. Valproate was partially effective for the epileptic spasms and focal seizures. Vigabatrin was effective for the epileptic spasms, but single spasms remained. A ketogenic diet was begun. The patient presented with severe developmental delay. After the administration of vigabatrin at 20 months of age, partial rolling over and eye contact were acquired.

Patient 5 is a 5-year-old female, who was the first child born to non-consanguineous Japanese parents. Fetal ultrasonography showed severe hydrops fetalis with ascites and right hydronephrosis. She was delivered at 37 weeks of gestation. Her birth weight was 3098 g (+1.5 SD), length 39 cm (−3.4 SD) and occipitofrontal circumference (OFC) 32.4 cm (−0.3 SD). Hydrops, congenital ascites and right hydronephrosis were noted. She showed respiratory distress at the neonate stage and failed to thrive because of feeding difficulties in infancy. She was mechanically ventilated and tube-fed for a considerable time. She manifested craniofacial dysmorphism including brachycephaly with wide fontanels, hypertelorism, short nose, cleft palate and micrognathia. She also showed arthrogryposis (congenital multiple joint contractures) with bilateral talipes equinovalgus. Radiological examination showed severe slenderness of tubular bones (gracile bones) with bowing of radii and fracture of the left femur. The ribs were also slender with a small thorax. Cranial CT demonstrated ventriculomegaly and partial premature fusion of both coronal sutures, with delayed calvarial ossification. Fractures of the right radius and right femur occurred in the neonatal period. Urological assessment revealed hypoplasia of the left kidney with a severe vesicoureteral reflux. The clinical phenotype suggested a diagnosis of osteocraniostenosis, but molecular analysis for *FAM111A* was negative.

She underwent tracheostomy at 1 month of age, vesicocutaneostomy for vesicoureteral reflux at 1 year, gastrostomy at 3 years of age and repair for cleft palate at 6 years of age. Mental development and physical growth were severely delayed. At 5 years, she could not roll over, sit alone or speak meaningful words. Height was 87 cm (−4.4 SD), body weight 10.2 kg (−2.9 SD) and OFC 53 cm (+1.9 SD). Cranial CT showed hydrocephalus and frontal plagiocephaly.

Patient 6 is a 7-year-old boy, who was the fourth child born to non-consanguineous healthy parents. He has two elder brothers and a sister. They are healthy with no seizure episodes. He was born by cesarean section at 37 weeks of gestation. Birth weight was 2815 g (−1.7 SD) and length 34 cm (−6.4 SD). Pedal edema was evident at birth. He obtained head control at 4 months of age, but sitting at 10 months, showing developmental delay. He could walk a couple of steps unaided at 4.5 years and speak two- and three-word sentences at 4.5 years. His DQ was 50 at the age of 4.5 years. He developed generalized seizures with fever at 5, 15 and 20 months. EEG showed abnormal background activity without epileptic discharge at 12 months and 4 years. His seizures were tractable and responded to lamotrigine, but abnormal background activity remained on EEG. Brain MRI showed periventricular white matter changes with asymmetric enlargement of the lateral ventricles (ventriculomegaly). He showed failure to thrive, short stature and microcephaly. At 4.5 years, his height was 85.0 cm (−5 SD), weight 10.0 kg (−4 SD) and head circumference 45.0 cm (−3.5 SD). In addition, he was clinically characterized by craniofacial and limb dysmorphic features including trigonocephaly, cleft palate, micrognathia, retrognathia, ptosis, arthrogryposis and brachydactyly.

WES analysis

WES was performed in all index patients and the parents of patients 1 and 5. DNA samples were captured by SureSelect^{XT} Human All Exon V5 or V6 (Agilent Technologies) and sequenced

on the Illumina HiSeq2500 with 101-bp paired-end reads (Illumina). Exome data processing, variant calling and annotation were performed as described previously (25,26). Average read depth of protein-coding regions ranged from 63× to 141×, and at least 92.9% of target bases were sequenced by ≥10 reads for each patient. Variants that fulfilled the following criteria were considered for further analysis: (1) variants with minor allele frequency < 0.1% in the Exome Sequencing Project (ESP6500), ExAC and our in-house Japanese exome database of 575 exomes; (2) possible pathogenicity based on mutation type (non-sense, missense, frameshift or splice site) with computational prediction of a deleterious protein function effect by SIFT, Polyphen-2, CADD and MutationTaster; and (3) *de novo* variants determined by subtracting variants found in either parent. Subsequently, *PPP3CA* variants were searched in our database of 1456 exomes of epilepsy patients as well as 1500 patients with various types of ID/MCA (*KDM1A* variants were also initially screened in 1456 exomes of epilepsy patients). All *PPP3CA* variants from each family were validated by Sanger sequencing regarding *de novo* occurrence.

PPP3CA expression analysis

In patient 4, total RNA was extracted from Epstein–Barr virus-transformed lymphoblastoid cells using RNeasy Plus Mini kit (Qiagen). cDNA was synthesized from 1 μg of total RNA and random hexamers using PrimeScript 1st strand cDNA synthesis kit (Takara). *PPP3CA* transcripts in a human multiple tissue cDNA panel (Clontech) were examined by PCR with primers at the exon 11–12 boundary (rt-F 11/12) and exon 14 (rt-R 14). Primer sequences are available on request. PCR included 35 cycles for qualitative splicing variant analysis, followed by electrophoresis in 2.5% agarose gels. Transcriptional variants 1 (NM_000944.4) and 2 (NM_001130691.1) were carefully examined by electrophoresis. For possible heteroduplex formation by different transcripts, a mismatch cleavage assay was performed using T7 endonuclease I (T7E1) to cleave heteroduplex DNA, in accordance with the manufacturer's instructions (New England Biolabs) (Supplementary Material, Fig. S5D).

Calculation of free energy change due to mutation

FoldX version 4.0 (9) was used to predict free energy change after mutation of the crystal structure of human calcineurin heterodimer (PDB code, 1AUI). RepairPDB, BuildModel and Stability commands implemented in FoldX software were used.

Yeast strains, media and growth conditions

For vegetative cell growth, rich media (YEA) or minimal media (EMM) were used with the addition of supplements as needed. Strains transformed with pREP1-expression plasmid (*LEU1*$^+$) were grown in EMM–leu agar plates to maintain plasmids. For serial growth dilution assays, cells were cultured at 32°C to a cell density of OD_{600} ~0.5 and collected by centrifugation. Cell density was adjusted to OD_{600} 0.5 and 1.0 for YEA and EMM agar plates, respectively. Ten-fold serial dilutions were spotted. Cells were grown for 3 and 5 days at 32°C in YEA and EMM agar plates, respectively. For Ca^{2+} sensitivity, $CaCl_2$ was added to YEA and EMM agar plates at a final concentration of 100 or 200 mM, respectively. FK506 (Tokyo Chemical Industry) and sodium valproate (Wako) were added to YEA agar plates at a final concentration of 0.5 μg/ml or 6 mM, respectively. Two independent experiments were performed for all serial growth dilution assays.

Plasmids

The *S. pombe* expression plasmid, pREP1, which has a thiamine-repressible *nmt1* promoter, was used to overexpress *ppb1* (27). Full-length *ppb1* cDNA (+1 to +1665) was obtained by reverse transcription (RT)-PCR and ligated into *NdeI* and *BamHI* restriction sites of pREP1. Site-directed mutagenesis using a KOD-Plus-Mutagenesis kit (Toyobo) was used to generate mutant *ppb1* (p.His121Arg, p.Asn179Ile, p.Asp263Glu, p.Phe499Leu and p.Ala502Thr), in accordance with the manufacturer's instructions, except using PrimeSTAR® HS DNA Polymerase (Takara).

Yeast strain construction

Strains expressing epitope-tagged proteins (Ppb1-HA and Prz1-GFP) under control of native promoters were constructed by a PCR-based method, as described previously (28). For constructing *ppb1* mutant alleles (Ppb1-HAHis121Arg, Ppb1-HAAsn179Ile, Ppb1-HAAsp263Glu, Ppb1-HAPhe499Leu and Ppb1-HAAla502Thr), the wild-type strain was transformed with a mutated *ppb1* DNA fragment fused to HA and a nourseothricin resistance cassette (29). *ppb1* mutations in the correct chromosomal locations were confirmed by Sanger sequencing.

Cell extract preparation and western blot analysis

Ten milliliter cultures at a cell density of OD_{600} 0.5 were used to prepare whole-cell extracts. Wild-type and mutant strains were exponentially grown in YEA medium and treated with 100 or 200 mM $CaCl_2$ for 30 min. In some cases, cells were pretreated with FK506 at a final concentration of 0.5 μg/ml. Whole-cell extracts were prepared using the glass bead method combined with trichloroacetic acid precipitation. For Prz1 mobility shift, whole-cell extracts were resolved on 4%–12% NuPAGE Bis-Tris Protein Gels (Invitrogen) in 1× NuPAGE SDS running buffer at a constant voltage of 200 V for 50 min, followed by western blotting. Anti-GFP (sc-9996; Santa Cruz Biotechnology), anti-HA (ab9110; Abcam) and anti-Cdc2 (sc-53217) were used for probing Prz1-GFP, Ppb1-HA and Cdc2, respectively.

Microscopy experiment

Live-cell imaging was performed on an FV1000-D confocal laser scanning microscope (Olympus) with a 60× 1.35 numerical aperture oil lens. Exponentially growing cells (OD_{600} ~0.5) were treated with 200 mM $CaCl_2$ for 30 min. Two independent experiments were performed in each strain with or without 200 mM $CaCl_2$.

RNA extraction and expression analysis for yeast

Total RNA was isolated from exponentially growing cultures using the Epicentre MasterPure Yeast RNA purification kit (Epicentre). cDNA was synthesized with 1 μg of total RNA and oligo dT primer using PrimeScript 1st strand cDNA synthesis kit (Takara). To quantify *pmc1* and *ncs1* expression, real-time quantitative PCR was performed. Rotor-Gene SYBR Green kit was used for real-time quantification of cDNA, with amplification monitored on the Rotor-Gene cycler system (Qiagen). Target gene expression was compared with that of an endogenous

control, actin (*act1*). Yeast strain transformed with empty vector was used as a calibrator sample for quantitation. For semi-quantification of *SPBPB21E7.04c* and *SPCC737.04* expression, RT-PCR products after 25 PCR cycles were analyzed using 2% agarose gels with ethidium bromide staining. Total RNA was independently extracted three times and subjected to real-time quantitative PCR and end-point RT-PCR analysis (in biological triplicates) except for the data shown in Supplementary Material, Figure S7C. Two independent experiments were performed for Supplementary Material, Figure S7C.

Web Resources

URLs for web resources:

- Exome Aggregation Consortium (ExAC) Browser, http://exac.broadinstitute.org/
- NHLBI Exome Sequencing Project (ESP) Exome Variant Server, http://evs.gs.washington.edu/EVS/
- SIFT, http://sift.jcvi.org/
- PolyPhen-2, http://genetics.bwh.harvard.edu/pph2/
- CADD, http://cadd.gs.washington.edu/home
- MutationTaster, http://MutationTaster.org/

All websites were last accessed on February 14, 2018.

GenBank accession numbers: *PPP3CA* cDNA, NM_000944.4; *ppb1* cDNA, NM_001022097.

Study Approval

This study was approved by the Institutional Review Boards of Yokohama City University School of Medicine and Showa University School of Medicine. All experiments were performed according to the respective approved protocols. Written informed consent was obtained from all participants.

Supplementary Material

Supplementary Material is available at *HMG* online.

Acknowledgements

We would like to thank all of the subjects and their families for participating in this study. We thank S. Grewal and the National BioResource Project (NBRP), Japan, for strains and reagents, and N. Watanabe and T. Sugiyama for technical assistance. We thank Rachel James, Ph.D., from Edanz Group (www.edanzediting.com/ac) for editing a draft of this manuscript.

Conflict of Interest statement. None declared.

Funding

This work was supported in part by a grant for Research on Measures for Intractable Diseases, a grant for Comprehensive Research on Disability, Health and Welfare, the Strategic Research Program for Brain Science (SRPBS) from the Japan Agency for Medical Research and Development (AMED), a Grant-in-Aid for Scientific Research on Innovative Areas (Transcription Cycle) from the Ministry of Education, Culture, Sports, Science and Technology of Japan (MEXT), Grants-in-Aid for Scientific Research (A, B, and C) and Challenging Exploratory Research from the Japan Society for the Promotion of Science (JSPS), the fund for Creation of Innovation Centers for Advanced Interdisciplinary Research Areas Program in the Project for Developing Innovation Systems from the Japan Science and Technology Agency (JST), the Takeda Science Foundation, grants from the Ministry of Health, Labour and Welfare, the Yokohama Foundation for Advancement of Medical Science and the Hayashi Memorial Foundation for Female Natural Scientists.

References

1. Rusnak, F. and Mertz, P. (2000) Calcineurin: form and function. *Physiol. Rev.*, **80**, 1483–1521.
2. Li, H.M., Rao, A. and Hogan, P.G. (2011) Interaction of calcineurin with substrates and targeting proteins. *Trends Cell Biol.*, **21**, 91–103.
3. Hashimoto, Y., Perrino, B.A. and Soderling, T.R. (1990) Identification of an autoinhibitory domain in calcineurin. *J. Biol. Chem.*, **265**, 1924–1927.
4. Yang, S.A. and Klee, C.B. (2000) Low affinity Ca^{2+}-binding sites of calcineurin B mediate conformational changes in calcineurin A. *Biochemistry*, **39**, 16147–16154.
5. Aramburu, J., Heitman, J. and Crabtree, G.R. (2004) Calcineurin: a central controller of signalling in eukaryotes. *EMBO Rep.*, **5**, 343–348.
6. Myers, C.T., Stong, N., Mountier, E.I., Helbig, K.L., Freytag, S., Sullivan, J.E., Ben Zeev, B., Nissenkorn, A., Tzadok, M. and Heimer, G. (2017) *De novo* mutations in *PPP3CA* cause severe neurodevelopmental disease with seizures. *Am. J. Hum. Genet.*, **101**, 516–524.
7. Unger, S., Gorna, M.W., Le Bechec, A., Do Vale-Pereira, S., Bedeschi, M.F., Geiberger, S., Grigelioniene, G., Horemuzova, E., Lalatta, F., Lausch, E. *et al.* (2013) *FAM111A* mutations result in hypoparathyroidism and impaired skeletal development. *Am. J. Hum. Genet.*, **92**, 990–995.
8. Kissinger, C.R., Parge, H.E., Knighton, D.R., Lewis, C.T., Pelletier, L.A., Tempczyk, A., Kalish, V.J., Tucker, K.D., Showalter, R.E., Moomaw, E.W. *et al.* (1995) Crystal structures of human calcineurin and the human FKBP12-FK506-calcineurin complex. *Nature*, **378**, 641–644.
9. Schymkowitz, J., Borg, J., Stricher, F., Nys, R., Rousseau, F. and Serrano, L. (2005) The FoldX web server: an online force field. *Nucleic Acids Res.*, **33**, W382–W388.
10. Yoshida, T., Toda, T. and Yanagida, M. (1994) A calcineurin-like gene *ppb1*+ in fission yeast: mutant defects in cytokinesis, cell polarity, mating and spindle pole body positioning. *J. Cell Sci.*, **107**, 1725–1735.
11. Hirayama, S., Sugiura, R., Lu, Y., Maeda, T., Kawagishi, K., Yokoyama, M., Tohda, H., Giga-Hama, Y., Shuntoh, H. and Kuno, T. (2003) Zinc finger protein Prz1 regulates Ca^{2+} but not Cl^{-} homeostasis in fission yeast. Identification of distinct branches of calcineurin signaling pathway in fission yeast. *J. Biol. Chem.*, **278**, 18078–18084.
12. McNamara, J.O., Huang, Y.Z. and Leonard, A.S. (2006) Molecular signaling mechanisms underlying epileptogenesis. *Sci. STKE*, **2006**, re12.
13. Hamasaki-Katagiri, N. and Ames, J.B. (2010) Neuronal calcium sensor-1 (Ncs1p) is up-regulated by calcineurin to promote Ca^{2+} tolerance in fission yeast. *J. Biol. Chem.*, **285**, 4405–4414.
14. Chatfield-Reed, K., Vachon, L., Kwon, E.J.G. and Chua, G. (2016) Conserved and diverged functions of the calcineurin-activated Prz1 transcription factor in fission yeast. *Genetics*, **202**, 1365–1375.
15. Popp, M.W. and Maquat, L.E. (2013) Organizing principles of mammalian nonsense-mediated mRNA decay. *Annu. Rev. Genet.*, **47**, 139–165.

16. Thomas, J.A., Rimoin, D.L., Lachman, R.S. and Wilcox, W.R. (1998) Gracile bone dysplasia. *Am. J. Med. Genet.*, **75**, 95–100.
17. Winslow, M.M., Pan, M., Starbuck, M., Gallo, E.M., Deng, L., Karsenty, G. and Crabtree, G.R. (2006) Calcineurin/NFAT signaling in osteoblasts regulates bone mass. *Dev. Cell*, **10**, 771–782.
18. Sun, L., Peng, Y., Zaidi, N., Zhu, L.L., Iqbal, J., Yamoah, K., Wang, X., Liu, P., Abe, E., Moonga, B.S. *et al.* (2007) Evidence that calcineurin is required for the genesis of bone-resorbing osteoclasts. *Am. J. Physiol. Renal.*, **292**, F285–F291.
19. Lindeboom, R.G., Supek, F. and Lehner, B. (2016) The rules and impact of nonsense-mediated mRNA decay in human cancers. *Nat. Genet.*, **48**, 1112–1118.
20. Chan, D., Weng, Y.M., Graham, H.K., Sillence, D.O. and Bateman, J.F. (1998) A nonsense mutation in the carboxyl-terminal domain of type X collagen causes haploinsufficiency in Schmid metaphyseal chondrodysplasia. *J. Clin. Invest.*, **101**, 1490–1499.
21. Wang, J., Gudikote, J.P., Olivas, O.R. and Wilkinson, M.F. (2002) Boundary-independent polar nonsense-mediated decay. *EMBO Rep.*, **3**, 274–279.
22. Buhler, M., Paillusson, A. and Muhlemann, O. (2004) Efficient downregulation of immunoglobulin mu mRNA with premature translation-termination codons requires the 5′-half of the VDJ exon. *Nucleic Acids Res.*, **32**, 3304–3315.
23. Pavone, P., Striano, P., Falsaperla, R., Pavone, L. and Ruggieri, M. (2014) Infantile spasms syndrome, West syndrome and related phenotypes: what we know in 2013. *Brain Dev.*, **36**, 739–751.
24. Arron, J.R., Winslow, M.M., Polleri, A., Chang, C.P., Wu, H., Gao, X., Neilson, J.R., Chen, L., Heit, J.J., Kim, S.K. *et al.* (2006) NFAT dysregulation by increased dosage of *DSCR1* and *DYRK1A* on chromosome 21. *Nature*, **441**, 595–600.
25. Saitsu, H., Nishimura, T., Muramatsu, K., Kodera, H., Kumada, S., Sugai, K., Kasai-Yoshida, E., Sawaura, N., Nishida, H., Hoshino, A. *et al.* (2013) *De novo* mutations in the autophagy gene *WDR45* cause static encephalopathy of childhood with neurodegeneration in adulthood. *Nat. Genet.*, **45**, 445–449.
26. Mizuguchi, T., Nakashima, M., Kato, M., Yamada, K., Okanishi, T., Ekhilevitch, N., Mandel, H., Eran, A., Toyono, M., Sawaishi, Y. *et al.* (2017) *PARS2* and *NARS2* mutations in infantile-onset neurodegenerative disorder. *J. Hum. Genet.*, **62**, 525–529.
27. Maundrell, K. (1993) Thiamine-repressible expression vectors pREP and pRIP for fission yeast. *Gene*, **123**, 127–130.
28. Bähler, J., Wu, J.-Q., Longtine, M.S., Shah, N.G., Mckenzie III, A., Steever, A.B., Wach, A., Philippsen, P. and Pringle, J.R. (1998) Heterologous modules for efficient and versatile PCR-based gene targeting in *Schizosaccharomyces pombe*. *Yeast*, **14**, 943–951.
29. Sugiyama, T., Cam, H., Verdel, A., Moazed, D. and Grewal, S.I. (2005) RNA-dependent RNA polymerase is an essential component of a self-enforcing loop coupling heterochromatin assembly to siRNA production. *Proc. Natl. Acad. Sci. U.S.A.*, **102**, 152–157.